Research Article

Ata El-kareim Shoeib, Ahmed Noureldean Arafa, Ahmed EL-sayed Sedawy*, and Awad M. EL-Hashmy

The shear strength of concrete beams hybrid-reinforced with GFRP bars and steel bars in main reinforcement without shear reinforcement

https://doi.org/10.1515/cls-2022-0013
Received Oct 07, 2021; accepted Feb 11, 2022

Abstract: The investigation of the structural performance of reinforced concrete members in the construction process has become a critical issue for Hybrid GFRP bars with steel bars. The ultimate concrete shear strength of reinforced concrete beams contains both GFRP bars and Steel bars in main reinforcement are a main task of work. This paper examines the effect of sharing the fiber-reinforced polymer (FRP) bars with steel bars for reinforced concrete (RC) structures on the concrete shear strength of RC beams. Fourteen RC beams without shear reinforcement were constructed and tested up to failure. The test beams included two steel-RC beams, one GFRP-RC beam, and eleven steel bars and GFRP bars (hybrid GFRP/steel)-RC beams. The main parameters were the reinforcement ratio, shear span to depth ratio, depth of the beam, concrete compressive strength, and compression reinforcement. The test results are presented in terms of crack patterns, failure modes, load-deflection, and load-strain behavior. The test results showed that hybrid GFRP/steel bars causing significant improvement in the ductility with reduction of the deformation comparing with an only steel bar in main steel in tested beams. The dowel action can play a major role in the process by which shear is carried in a beam. Finally, the initial proposal equation that calculates the shear strength of hybrid reinforced elements can serve as a guideline for the introduction of hybrid bars (GFRP and Steel) at the main reinforcement in RC beams.

Keywords: Hybrid steel bars with GFRP bars in main reinforcement, reinforcement ratio, shear span-to-depth ratio, depth of the beam, and concrete compressive strength

Notation list

ϕ	the diameter of steel
#	the diameter of the fiber
ρ	the percentage of reinforcement
c	the concrete cover
d	the effective depth
x_1	the distance of the diagonal crack from the beam support
f_c	the concrete compressive strength
c_s	the side cover
c_i	the horizontal distance between consecutive bars
f_{ct}	the concrete tensile strength
bn	the net width of the beam ($b - n\varnothing$)
nb	the number of bars in one layer
c_m	the minimum cover (side or bottom)
V_{cf}	shear capacity of concrete beams without shear reinforcement
E_r	modulus of elasticity of reinforcement
b_w	width of the web in mm
f_c	concrete compressive strength
E_f	modulus of elasticity FRP
E_s	modulus of elasticity steel
b	width of beam
M_f	factored moment
V_f	the factored shear

1 Introduction

Numerous studies have been carried out to evaluate the performance of using FRP bars to substitute steel bars to solve the durability problem of reinforced concrete structures in an aggressive environment, such as bridges' decks and roadbeds which may encounter serious corrosion of

***Corresponding Author: Ahmed EL-sayed Sedawy:** Faculty of Engineering Mataria, Helwan University, Helwan, Egypt; Email: ahmedsedawy1@gmail.com
Ata El-kareim Shoeib, Awad M. EL-Hashmy: Faculty of Engineering Mataria, Helwan University, Helwan, Egypt
Ahmed Noureldean Arafa: Faculty of Engineering, Sohag University, Sohag, Egypt

steel reinforcement [1–3]. Moreover, the lifespan of FRP materials has been demonstrated to be much longer than that of traditional steel reinforcement. It is reported that the embodied energy of FRP is 68% lower than that of steel [4]. Due to these characteristics, FRP can be considered as a sustainable construction material with less environmental effect compared to steel. Despite the above-mentioned benefits, FRP exhibits a linear elastic behavior up to failure and has little ductility in general compared to steel bars, which is a drawback when it serves as internal reinforcement in concrete structures [5–7]. various researchers have experimentally studied the design of adding steel bars to FRPRC beams, to improve the ductility of FRP reinforced concrete (FRPRC) [8, 9]. Bui *et al.* [2] investigated the ductility of FRP/steel RC beams by taking into account the effects of the FRP reinforcement position on the mechanical performance of the beams as well as the effects of the fiber-reinforced polymer on the steel reinforcement ratio. The results of this study revealed that ductility defined by absorption energy differed from ductility measured by conventional steel RC beams. Maranan *et al.* [6] also showed that there was a ductility contradiction between displacement ductility and energy-based ductility, with the increase in displacement ductility leading to a decrease in energy absorption. In a hybrid reinforcement scenario, the strength can be mainly provided by FRP reinforcement and the ductility can be provided by the addition of steel reinforcement. Since the additional steel reinforcement is not designed for the load-bearing capacity of the beam. Moreover, the deformation and the crack width of hybrid FRPRC beams are reduced compared to those of pure FRPRC beams [10–13]. A large number of tests on steel or FRP-reinforced concrete members without shear reinforcement have been carried out to quantify (V_c) [14–24]. This resulted in developing multiple formulas for predicting the concrete shear contribution in steel or FRP-reinforced elements [25–34]. Yet, due to the absence of experimental studies on the behavior of hybrid reinforced elements, no equations have been developed to predict the shear response of such structural elements.

The GFRP bars are considerably different from steel, owing to their substantially lower elasticity modulus and binding to concrete behaviour, which is heavily influenced by surface preparation. Due to the tensile stress transmission from the concrete matrix to the reinforcement, the performance of FRP reinforced concrete necessitates an appropriate interfacial connection between the bars and the concrete. Stress propagation ensures bond-slip contact between the FRP bar and surrounding concrete, which is dependent on the geometry of the bar, mechanical interaction, chemical adhesion, and frictional forces, as well as the compressive strength of concrete. The nominal diameter of the bars, the concrete cover, the kind of FRP bar, it's surface preparation, bond length, and concrete strength all have a significant impact on the bond behaviour of the FRP reinforcement to concrete. There has been a lot of study on the bond behaviour of FRP reinforcement to concrete, mostly using the direct pull-out test, beam test, splice test, and ring pullout test [35–41]. The bar's ultimate bond stress (t_u) is defined as the average bond shear stress over the embedded length and can be determined using the following equation:

$$t_u = \frac{F_u}{\pi.\varnothing.L_b}$$

where F_u is the pull-out force, φ is a nominal bar diameter and L_b is the embedded bond length. The increase in a slip-loaded end SLP and bond length Lb in ribbed bars is greater than in sand-coated bars [42]. Furthermore, the bond stiffness and shear stress of the ribbed bars are larger than those of the sand-coated bars [40]. The shear bond stress and ultimate bar slip were both reduced as the bar diameter was increased. Many researchers [43–46] have conducted comprehensive experimental experiments focused on the shear failure of reinforced concrete beams over the last two decades to capture the failure causes. As a result, many shear failure models were presented in an attempt to obtain suitable equations for designing engineers to forecast the shear strength of reinforced concrete beams with high precision. However, the calculations utilised in various design codes are empirical because there is no physically sound analytical model that can produce adequate results for all scenarios of shear failure of reinforced concrete beams. In recent years, some researchers have focused on the application of fracture mechanics to the shear failure of reinforced concrete beams without stirrups to establish an analytical model with a solid physical foundation. This is based on the notion that the shear failure of a beam is caused by a sequence of fractures.

Predicting the shear strength of R.C. beams in different types of material bars is critical for their safe design and acceptance of hybrid FRP/steel as reinforcement. Despite numerous investigations dedicated to evaluating the shear strength of pure steel or pure fiber bars in R.C. beams, fewer studies have been conducted on the assessment of the shear strength in the case of Hybrid GFRP bar with steel bars (hybrid) in the main reinforcement of the R.C beams. This has been the main impetus to carry out this study to fill this gap of knowledge and provide information about this behavior. The effect of using hybrid reinforced elements is studied taking the following items into account: the type of reinforcing bars, reinforcement configuration and ratios, size effect, shear span-to-depth ratio, and concrete strength.

2 Experimental program

This study included testing and analysis of fourteen tested RC beams with rectangular cross-sections, sized 120 mm (width) × variable (height) × 2300 mm (length). The details of the tested specimens are shown in Figure 1. In this work, when the main reinforcement is combined between GRFP bars and Steel bars the tested specimens are defined as hybrid GFRP/steel RC tested specimens.

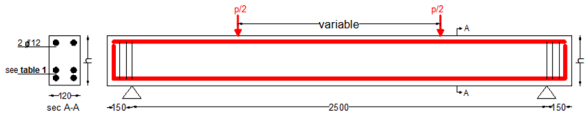

Figure 1: Details of a typical specimen

The tested RC beams were divided into fifth groups; Group one study the behavior of pure steel reinforcement beams and pure GFRP reinforcement beams. two RC tested beams with bottom steel bars (4ϕ10, 4ϕ12), And one RC tested beam with GFRP bars (4#4). Group two study the reinforcement configuration and ratios have three tested beams with bottom reinforcement (2ϕ10, 2#3), (2ϕ12, 2#4), and (2ϕ10, 2#5). The third group study size effect, and has two tested RC beams with depth(200mm,400mm), bottom reinforcement (2ϕ12, 2#4).

The fourth group examines the effect shear span-to-depth ratio and has three tested RC beams with, span-to-depth ratio equal to (2, 3, and 4), bottom reinforcement is (2ϕ12, 2#4). The fifth group studies concrete strength, and has three tested RC beams with concrete strength (30Mpa, 40Mpa, 50Mpa), depth 300mm, bottom reinforcement (2ϕ12, 2#4), and span to depth ratio 2.67.All beams top reinforcement (2ϕ10). Details of the tested beams with different parameters are shown in Table 1.

2.1 Manufacturing and testing of plain concrete

The concrete mix used to cast the RC beams consisted of aggregates, Portland cement, and natural water. The type of cement used was Portland cement CEM-I42.5N. Coarse aggregate was crushed dolomite with a maximum particle size of 12.50 mm. Mixing was performed using a concrete tilted rotating drum mixer with a maximum capacity of 0.125 m^3. Dolomite, sand, and cement were dry mixed. Then, water was progressively added, as the concrete mixed for an additional two minutes, after which the concrete became homogeneous. The concrete was cast in molds and moist burlap sheets covering the specimens until ready for testing.

2.2 Manufacturing and testing vars

The GFRP bars were made locally by glass fiber roving. Double sets of plastic mold were manufactured at a special workshop that manufactures variable long GFRP bars with 10mm, 12mm, and 16mm diameter as shown in Figure 2. The tensile average strength of GFRP bars was equal to 505

Table 1: The experimental program and results

	Specimen no	h (mm)	Reinf. steel	Reinf. GFRP	AS′	a/d	f_c (Mpa)	First crack load Pcr (KN)	Failure load Pu (KN)	Maximum load Pmax (KN)	Deflection at pmax
G1	B1	300	4ϕ10	––	2ϕ12	2.67	25	39.5	20.8	82.8	5.771
	B2	300	4ϕ12	––		2.67	25	64.5	30.7	92.8	5.319
	B3	300	––	4#4		2.67	25	17.5	35.8	51.3	8.609
G2	B4	300	2ϕ10	2#3		2.67	25	21.84	38.4	67.84	6.164
	B5	300	2ϕ12	2#4		2.67	25	37.4	25	73.2	5.951
	B6	300	2ϕ12	2#5		2.67	25	40.7	23	105.7	6.95
G3	B7	200	2ϕ12	2#4		2.67	25	48.2	34.3	65	5.996
	B8	400	2ϕ12	2#4		2.67	25	41.3	13.2	99.3	6.37
G4	B9	300	2ϕ12	2#4		2.0	25	37.7	21.1	75.6	5.154
	B10	300	2ϕ12	2#4		3.0	25	24.8	24.5	59.8	6.018
	B11	300	2ϕ12	2#4		3.5	25	23.7	12.9	53.4	7.067
G5	B12	300	2ϕ12	2#4		2.67	30	40.5	23	78.9	5.73
	B13	300	2ϕ12	2#4		2.67	40	49	18.3	103.2	5.563
	B14	300	2ϕ12	2#4		2.67	50	64.8	8.4	126.4	4.804

(ϕ) the diameter of steel, and (#) the diameter of the fiber

#3 equals to 10 mm, #4 equals to 12 mm, and #5 equals to 16 mm

Table 2: The ductility index and area energy absorption of tested RC beams

	Specimen no	h (mm)	Reinf. steel	Reinf. GFRP	a/d	f_c (Mpa)	Maximum load Pmax (kN)	ΔMax	Δfailure	Ductility index =Δfailure/ΔMax	Area under P-d
G1	B1	300	4ϕ10	—–	2.67	25	82.8	5.771	7.474	1.295	393.6433
	B2	300	4ϕ12	—–	2.67	25	92.8	5.319	6.69	1.257	396.2522
	B3	300	—–	4#4	2.67	25	51.3	8.609	9.469	1099	315.2754
G2	B4	300	2ϕ10	2#3	2.67	25	67.84	6.164	6.994	1.134	335.9676
	B5	300	2ϕ12	2#4	2.67	25	73.2	5.951	7.626	1.281	384.9197
	B6	300	2ϕ12	2#5	2.67	25	105.7	6.95	12.621	1.816	834.21
G3	B7	200	2ϕ12	2#4	2.67	25	65	5.996	6.8	1.281	265.57
	B8	40	2ϕ12	2#4	2.67	25	99.3	6.37	7.058	1.108	423.3834
G4	B9	300	2ϕ12	2#4	2.0	25	75.6	5.154	8.127	1.576	391.7413
	B10	300	2ϕ12	2#4	3.0	25	59.8	6.018	8.931	1.484	342.59
	B11	300	2ϕ12	2#4	3.5	25	53.4	7.067	8.952	1.266	320.7889
G5	B12	300	2ϕ12	2#4	2.67	30	8.9	5.73	7.428	1.296	412.6021
	B13	300	2ϕ12	2#4	2.67	40	103.2	5.563	7.90	1.420	504.30
	B14	300	2ϕ12	2#4	2.67	50	126.4	4.804	9.184	1.911	627.3329

Figure 2: Shape of GFRB bars

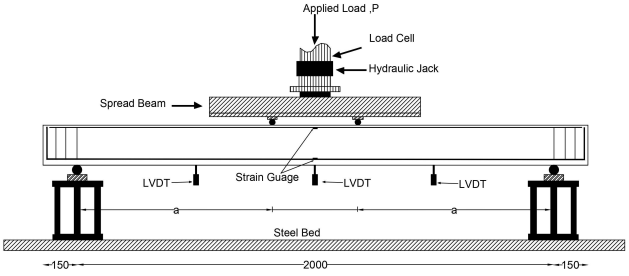

(a) Sketch of an experimental test set-up

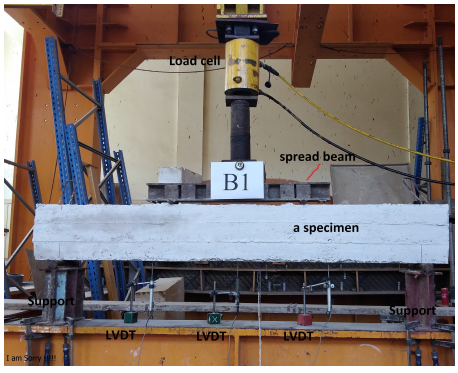

(b) Test set-up photo

Figure 3: Experimental test setup

MPa with a corresponding strain equal to 0.055 mm. The manufacture steel-reinforced concrete had 360 MPa yield strength for main and secondary steel reinforcement.

3 Experimental setup and testing

The beams were tested using a hydraulic jack with a capacity of 1000 kN, manually powered by an oil pump. The test setup and instrumentation used are shown in Figure 3. An electrical load cell with an accuracy of 0.1 kN connected to a digital load indicator is used to calculate the applied vertical loads. The deflection of the tested beams was recorded using three electric dial gauges LVDT, one at mid-span, and the others located at quarter-span from each support of the tested beam located at the bottom surface of the beam supports. The strain of the main fiber, steel reinforcement were measured using two strain gauges. The three electric dial gauges, load cell, and two electric strain gauges were attached to the data acquisition system connected to the computer. Continuous recording of the load, displacements, and reinforcement strains were recorded during each test beam up to failure.

4 Test results and analysis

Tables 1 and 2 show the experimental results of the tested RC beams, and Figures 4–7 show the behavior of tested RC beams for different parameters. The load-deflection curves, crack patterns and mode of failures, and the strain in the main GFRP/steel bars at the mid-span section are presented.

4.1 Crack patterns and modes of failure

The crack patterns and modes of failures of the tested RC beams are shown in Figure 4. In general most of the cracks were found in the shear zone and prolonged in the direction of the compression zone causing all beams failure in the shear. Some cracks formed in the moment zone and their length increased together with an increase in the load until beam failure occurs.

A comparison of cracks formed in tested RC beam with pure steel (B2), beam with pure fiber (B3), and beam with hybrid (B5), found that the number and width of cracks increased when fiber was used. However, using hybrid beams decreased the number and width of cracks compared to using pure steel or pure fiber.

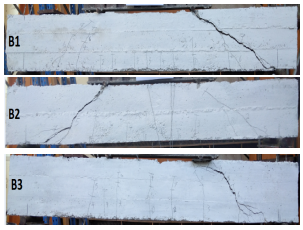

(a) The crack patterns for group (G1)

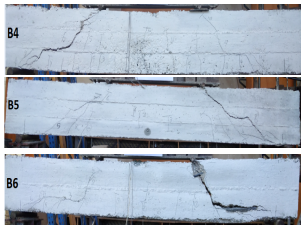

(b) The crack patterns for group (G2)

(c) The crack patterns for group (G3)

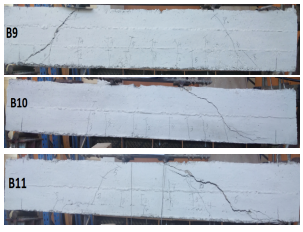

(d) The crack patterns for group (G4)

(e) The crack patterns for group (G5)

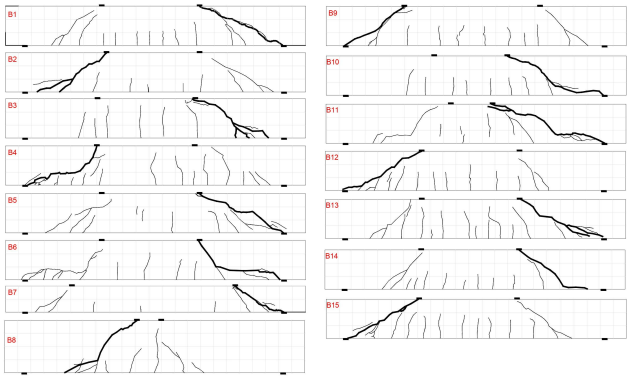

Figure 4: The crack patterns of tested specimens

For groups (G1, G2) which studied using different reinforced bars with different reinforcement ratios, the study showed that more cracks appeared on the shear zone and that the number of flexural cracks decreased together with an increase in the reinforcement ratio, the number and width of cracks decreased when hybrid bars were used compared with steel or fiber bars. Additionally, the number of cracks decreased with an increased diameter bar as shown in Figures 4a and 4b, also the sound of failure of hybrid beams such as beams reinforced with steel bars but no sound occurs during failure on beams reinforced with GFRP only. A comparison of cracks formed in tested RC beams variable depth 200 mm, 300 mm, and 400 mm, found the cracking load and the number of cracks decreased when the depth of the beam is decreased. Group G4 studied the effect of span -to- depth ratio. Figure 4d shows that by increasing span-to-depth ratio, the crack width increased while the number of cracks goes down. The crack patterns for group G5 show a decrease in the number and width of cracks when the concrete strength is increased.

A comparison of cracking load in tested RC beam with pure steel (B2), beam with pure fiber (B3), and beam with

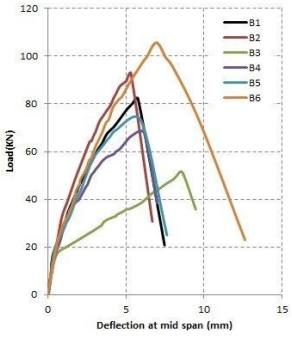

(a) Load-deflection curve for reinforcement ratio and configuration effect

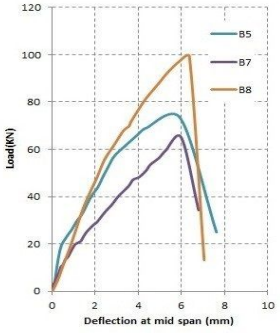

(b) Load-deflection curve for variable depth effect

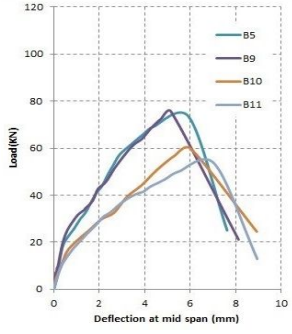

(c) Load-deflection curve for span -to- depth ratio effect

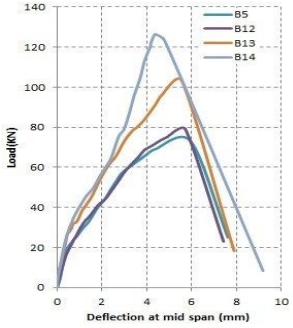

(d) Load-deflection curve for concrete strength effect

Figure 5: Load-deflection curve at mid-span curves

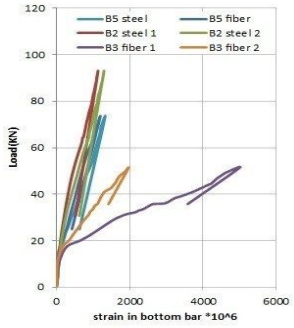

(a) Load-strain curve for reinforcement ratio and configuration effect

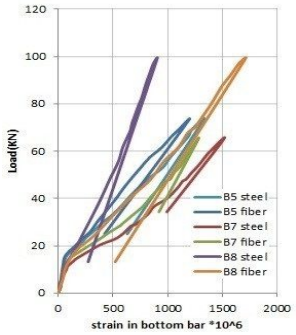

(b) Load-strain curve for variable depth effect

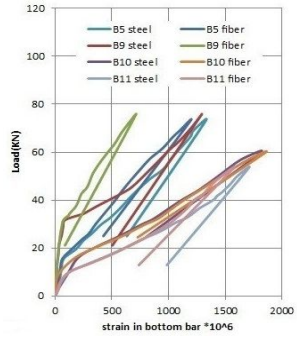

(c) Load-strain curve for -to-depth ratio effect

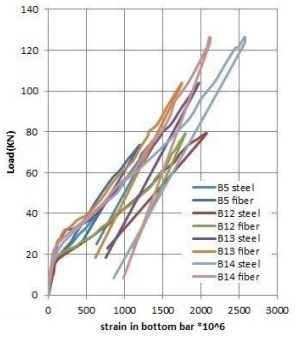

(d) Load-strain curve for concrete strength effect

Figure 6: Load-strain curve at mid-bottom steel

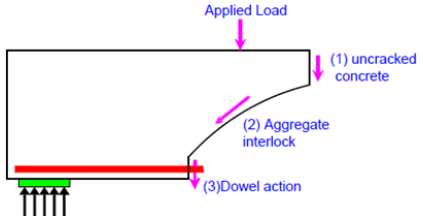

Figure 7: Mechanism of shear transfer in a cracked concrete beam

hybrid GFRP/steel, were 64.5kN, 17.5 kN, and 37.4 kN respectively. The point is that the cracking load in pure steel increased by 260% more than pure fiber, the cracking load in hybrid beams decreased by 70% less than pure steel but, the cracking load in hybrid beams increased by 110% more than pure fiber. As a result, we can say that using hybrid and pure steel delayed cracking appearance more than pure fiber.

In the first and second group, the cracking loads for tested specimens, beam with steel diameter 10 mm (B1), beam with steel diameter 12 mm (B2), beam with hybrid GFRP/steel diameter 10 mm (B4), and beam with hybrid diameter 12 mm (B5) were 39.5 kN, 64.5 kN, 21.84 kN, and 37.4 kN, respectively. Consequently, we observed approximations ranging from 35% to 70% of cracking loads reduction when using GFRP with steel. We also found that the cracking load goes down when the depth of beams increased. Comparing the cracking load for beams with variable span-to-depth ratios (2, 2.67, 3 and 3.5) were 37.7 kN, 37.4 kN,24.8 kN, and 23.7 kN, we found that the cracking load decreased when span- to- depth ratio increased delayed cracking appearance. The crack patterns for group G5 are revealed in Figure 4e. When the concrete strength was increased, the cracking loads were 40.5 kN, 49kN, and 64.8 kN respectively. For this reason, we concluded that increasing concrete strength caused the cracking load to reduce, however, the width of cracks increased. Finally, cracks and mode of failure in hybrid beams are closer to beams with steel bars than to beams reinforced with GFRP only.

4.2 Load deflection curves

A comparison of maximum deflection in tested RC beam with pure steel (B2), beam with pure fiber (B3) and beam with hybrid, were 5.319 mm, 8.609 mm, and 5.951 mm respectively and maximum load were 92.8 kN, 51.3 kN, and 73.2 kN respectively from this the maximum load in pure steel increased by 80% and deflection decreased by 62% compared to pure fiber, the maximum load in hybrid beams decreased by 26% and deflection increased by 11% compared to pure steel but, the maximum load in hybrid beams increased by 42% and deflection decreased by 45% compared to pure fiber. From this, we can say using a hybrid beam increased load and decreased deflection compared to pure fiber.

As shown in Figure 5a, we found that the maximum deflection increased with a used GFRP bar where the max deflections were equal to 5.771 mm and 5.319 mm for tested beams reinforced with a steel bar, 8.609 mm for beam reinforced with GFRB bar only, 6.164 mm and 5.951 mm for tested beams reinforced with hybrid steel/GFRP bar. From load-deflection curves, we found that the beams reinforced with hybrid GFRP/steel decreased the deflection of RC beams reinforced with GFRB bar only and caused increasing the maximum load. By using variable depth 200 mm, 300 mm, and 400 mm, the maximum load were 65 kN, 73.2 kN, and 99.3 kN, respectively, causing increased maximum loads, The influence of span- to- depth ratio on the load-deflection curves as shown in Figure 5c, the maximum deflection for tested specimens a/d (2, 2.67, 3 and 3.5) were equal to 5.154 mm, 5.951 mm, 6.018 mm and 7.067 mm, respectively. From this, we concluded by increasing a/d the ductility and maximum loads decreased, and maxi-

mum deflection increased so a/d equals 2 is the best ratio because it gave good results compared to other ratios. Also, Figure 5d shows increasing the concrete strength works to reduce deflection; therefore increasing concrete strength has a very important and fundamental role in improving the behavior of the beams in general.

4.3 Stiffness and energy absorption

Energy absorption is defined as the area under a load-deflection curve. In general, load-deflection curves in Figure 5 shows that the energy absorption increased by using hybrid bars compared with GFRP bars. A comparison of energy absorption in tested RC beam with pure steel (B2), beam with pure fiber (B3) and beam with hybrid, were 396.25, 315.27, and 384.91, respectively. In other words, the energy in pure steel increased by 25% more than pure fiber, the energy in hybrid beams decreased by 2% less than pure steel but, the cracking load in hybrid beams increased by 23% more than pure fiber. To conclude, we can say that using hybrid and pure steel enhances energy more than pure fiber.

As for the first group, that's to say the beams with pure steel: the energy for tested specimens with a diameter (10 mm, 12mm) was equal to 393.64 and 396.25, respectively, and the energy for a beam with GFRP only was equal to 315.27. On the other hand, the second group, with hybrid, GFRP/steel the energy for tested specimens with diameter 10 mm, 12mm and 16 mm were equal to 335.96, 384.91, and 834.21, respectively. For this reason, we concluded that using GFRP with steel may enhance the energy especially when the reinforcement ratio of hybrid bars increased. To put it another way, on using variable depth 200 mm, 300 mm, and 400 mm, the energy increased by 10%-27% as shown in Table 2. The influence of span-to-depth ratio and the energy for tested specimens with a\d (2,2.67,3 and 3.5) were equal to 391.74,384.91, 342.59, and 320.78, respectively. That's why, we concluded that when we increased a/d the energy decreased by 1%-18%. Finally, Figure 5e, shows that the effect of concrete strength: when the concrete strength is increased, the energy goes up by 7%-63%.

A beam's stiffness indicates its ability to return to its original shape or form after an applied load is removed (ratio between the load to deflection), A comparison of stiffness in tested RC beam with pure steel (B2), beam with pure fiber (B3), and beam with hybrid, were 17.45, 5.96, and 12.3, respectively from this the stiffness in pure steel is more than pure fiber, the stiffness in hybrid beams is less than pure steel but, the stiffness in hybrid beams are more than pure fiber. From this, we can say using hybrid and pure steel enhance the stiffness more than pure fiber.

The stiffness of tested specimens increased when the reinforcement ratio of bars was increased as shown in Figure 5a. Besides, As shown in Figure 5b, it is clear that by using variable depth the stiffness of tested specimens with depth 400 mm is more than that of the stiffness of tested RC beams with depth 200 mm and 300 mm. As shown in Figure 5c, it can be observed that by using variable span to depth ratio, the stiffness increased when span-to-depth ratio decreased, so a\d equals 2 gave more stiffness than a\d equals 2.67, 3 and 3.5. Finally, Figure 5d showed that the stiffness of tested RC beams with compressive strength (30, 40, and 50) are more than compressive strength 25.

4.4 Ductility

The ductility of RC beams is the ratio between the deflections at the failure to deflection at the maximum loads. A comparison of ductility in tested RC beam with pure steel (B2), beam with pure fiber (B3) and beam with hybrid, were 1.257, 1.099 and 1.281, respectively. From this the ductility in pure steel increased by 14% more than pure fiber, the ductility in hybrid beams increased by 2% more than pure steel but, the cracking load in hybrid beams increased by 16% more than pure fiber. From this, we can say using a hybrid beam enhance the ductility more than pure fiber.

For group one, reinforced with steel, the ductility index for tested specimens with a diameter of 10mm and 12 mm were equal to 1.295, and 1.257, respectively. On the other side, for group two, with hybrid GFRP/steel the ductility index for tested specimens with diameter 10mm, 12mm, and 16mm were equal to 1.134, 1.281, and 1.816, respectively. From this, we concluded that using GFRP with steel may enhance ductility. By using variable depth 200 mm, 300 mm, and 400 mm, the ductility induced were 1.134, 1.281, and 1.108, respectively, causing a slight effect on the ductility. The influence of span-to-depth ratio on the load-deflection curves as shown in Figure 4c, the ductility index for tested specimens a\d (2, 2.67, 3, and 3.5) were equal to 1.576, 1.281, 1.484, and 1.266, respectively. From this, we concluded by increasing a/d the ductility decreased. Also, Figure 5e, shows the effect of concrete strength and that increasing the concrete strength works to improve ductility and reduce deflection.

4.5 Main reinforcement strain at mid-span

The load-strain curves of the tested RC beams were presented in Figure 6. In general, from the figure, it is found

that the maximum strains for steel bars at the mid-span section were between 0.9% and 2.5%, knowing that the yield strain and the ultimate strain of steel used (12 mm diameters) were equal to 1.8%, and 2.7%, respectively. From this, we concluded that the tensile stress of the main steel bar reached and also exceed the yield strain of steel bars because of the beams without stirrups. Also, it found that the maximum strains for fiber bars at the mid-span section were between 0.7% and 2.1% in beams reinforced with hybrid, and fiber reached 4.99% in beams reinforced with FRP only due to using hybrid decreased the strain in the bars. By comparison strain in GFRP equal approximately 85% from strain in steel. From this, we concluded that the GFRP bar plays the same role as the steel of resistive loads. With increasing the depth of the beam, the strain in the bar increases, and the strain in the bar decreased when the span-to-depth ratio equals 2 and the concrete strength is increased, the bars get close to ultimate strain. From this, we understand that the effect of tension hybrid reinforced testing RC beams has an important role in resistance loads. There is a match in the strain of steel and fiber values in most hybrid beams.

5 Theory studied

In a reinforced concrete beam without shear reinforcement, the internal shear force is currently assumed to be resisted by the uncracked concrete (V_c), aggregate interlock (V_a), and dowel action (V_d) as shown in Figure 7. This paper focuses on the dowel action because the main objective evaluates the ultimate shear strength with hybrid main reinforcement of RC beam.

5.1 Fracture mechanics

It was widely assumed that shear failure of reinforced concrete beams is intimately related to a succession of fracture processes and has a significant size effect. Previously, several existing models with some physical meaning based on such intensive investigations on the shear failure of reinforced concrete beams without stirrups only captured a small portion of the interpretation for the shear mechanisms in both physics and mathematics. These studies primarily include Bazant's size effect formula [32], Gustafsson and Hillerborg's numerical stimulation using fictitious crack model [43] Jenq and Shah's diagonal shear crack analysis based on two-parameter fracture model [44] Karihaloo's modification [45] for Jenq and Shah's model, and Gastebled and May's analytical model by a fracture energy approach [46]. A more detailed description of Gastebled and May's shear fracture principle and accompanying calculation expressions is provided for the sake of convenience and clarity in deducing new analytical formulas in the sequence section.

5.1.1 Proposed analytical formula

Shilang Xu devired equation to predict the shear bearing capacity of reinforced concrete beams without stirrups is anew obtained using fracture toughness K_{IIC} as follows

$$V_c = \frac{0.446}{\sqrt{H}}\sqrt{\frac{E_s}{E_c}}\left(\frac{H}{a_s}\right)^{0.33}\rho^{\frac{1}{6}}(1-\sqrt{\rho})^{.67}K_{IIC}bH \quad (1)$$

as steel

$$V_c = \frac{0.446}{\sqrt{H}}\sqrt{\frac{E_f}{E_c}}\left(\frac{H}{a_s}\right)^{0.33}\rho^{\frac{1}{6}}(1-\sqrt{\rho})^{.67}K_{IIC}bH \quad (2)$$

as fiber

$$V_c = \left[\frac{0.446}{\sqrt{H}}\left(\frac{H}{a_s}\right)^{0.33}\rho^{\frac{1}{6}}(1-\sqrt{\rho})^{.67}K_{IIC}bH\right] \cdot \left[\frac{\sqrt{E_s}+\sqrt{E_f}}{\sqrt{E_c}}\right] \quad (3)$$

The corresponding comparison results are shown in Table 3.

As shown in Table 3, the proposed equation gives acceptable results compared with the CSA.

Table 3: The shear bearing capability calculated using several formulae

	CSA S806-02	Proposed equation	Proposed/CSA
B4	3.1	3.0	0.97
B5	4.09	4.05	0.99
B7	2.6	2.67	1.02
B8	5.5	5.3	0.96
B9	4.2	4.25	1.01
B10	3.6	3.7	1.02
B11	3.47	3.5	1
B12	4.3	4.25	0.99
B13	4.8	4.7	0.98
B14	5.2	5.3	1.02

5.2 Dowel action

The dowel force is caused by the contact between the bars and the surrounding concrete. when the reinforcement bars resist forces perpendicular to their axis. Yielding of the bar and concrete crushing under the dowel, and concrete splitting are two failure modes that occurred under the dowel action mechanism depending on the concrete strength, bar diameter, and concrete cover [24–27]. However, the equations did not take into account the various bar materials and strengths. The experimental program consisted of four specimens with the same dimensions and the same main reinforcement, but they had different shear plane reinforcement. Figure 8 shows the specimen dimensions, the main steel, and the shear reinforcement details.

The first specimen with steel in shear reinforcement and the other specimen with GFRP with different diameters (#3, #4, #5). The results obtained from the direct shear tests are summarized in Table 4. Figure 9 shows modes of failure in tested specimens with steel bars and fiber bars. The experimental testing of the specimens showed that the type of bar materials and properties is very important for calculating the dowel action force.

From this, we concluded that the shear strength of GFRP bar approximately equals 40% of steel bar.

Many researchers have performed experiments to examine the strength of the dowel when the mode of failure is due to the splitting of concrete, so there are only empirical formulas available. Table 5 shows some of the expressions proposed for the prediction of the dowel force (V_d):

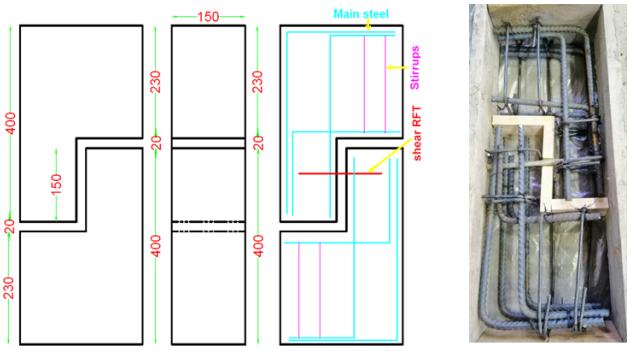

Figure 8: Dowel action test, sample details (dimensions and reinforcement). All dimensions are in mm

Figure 9: Dowel action samples (failure modes)

Table 4: Results of dowel action test

Type		GFPP		steel
Diameter(mm)	#3 (10mm)	#4 (12mm)	5# (16mm)	12mm
Shear strength(KN)	284	567	1135	1367

Table 5: Some equations for prediction of the dowel force

1 – Krefeld and Thurston [35]	$V_d = b\sqrt{f_c}\left[1.30\left(1+\frac{180\rho}{\sqrt{f_c}}\right)c+d\right]*\frac{1}{\sqrt{(x_1/d)}}$
2 – Taylor [36]	$V_d = 9.1 + 0.0001[\sum(c_s + c_i)]^2 f_{ct}$
3 – Houde and Mirza [37]	$V_d = 37 b_n \sqrt[3]{f_c}$
4 – Jimenez, Gergely and White [38]	$V_d = \frac{b_n d_b}{n_b}\left(3.25+\frac{3.79 c_m}{\frac{b_n}{n_b^2}+d_b}\right)$
5 – Baumann and Rüsch [42]	$V_d = 1.64 b_n \varnothing^3 \sqrt{f_c}$

ρ: is the percentage of reinforcement, c: is the concrete cover, d: is the effective depth, x_1: is the distance of the diagonal crack from the beam support, f_c: is the concrete compressive strength, c_s: is the side cover, c_i: is the horizontal distance between consecutive bars, f_{ct}: is the concrete tensile strength, bn: is the net width of the beam ($b - n\varnothing$), nb is the number of bars in one layer, c_m: is the minimum cover (side or bottom)

Table 6: Shear capacity of concrete beams reinforced with FRP bars without shear reinforcement

Design procedure – FRP (researchers)	Calculations
Tottori and Wakui [13]	$V_{cf1} = 0.2(f'_c)^{\frac{1}{3}}\left(\rho_f^{\star}\right)^{\frac{1}{3}}\left(\frac{1000}{d}\right)^{1/4}\left[0.75 + \frac{1.4}{(a+d)}\right]bd$ $V_{cf2} = 0.244(f'_c)^{\frac{2}{3}}\left(1 + \sqrt{\rho_f^{\star}}\right)\left(\frac{[1+3.33(r/d)]}{[1+(a/d)^2]}\right)bd$ Where $\rho_f^{\star} = \rho_f(\frac{E_f}{E_s})$ V_{cf} as the larger of V_{cf1} and V_{cf2}
Zhao *et al.* [14]	$V_{cf} = 0.2\left(1 + \beta_p + \beta_d\right)\left[0.75 + \frac{1.4}{(a+d)}\right](f'_c)^{1/3}bd$ *Where* $\beta_p = \left(100\rho_f^{\star}\right)^{1/2} - 1 \le 0.73$ $\beta_d = \left(100\rho_f^{\star}\right)^{1/4} - 1$
Tureyen and Frosch [15]	$V_{cf} = 0.415\sqrt{f'_c}bc$ $c = kd \quad k = \sqrt{2\rho_n + (\rho_n)^2} - \rho_n \quad n = E_r/E_c$
Hegger *et al.* [27]	$V_c = k_f \cdot \beta \cdot 0.205 \cdot k \cdot \left(100 \cdot \rho_f \cdot \frac{E_f}{E_s} \cdot f_c\right)^{\frac{1}{3}} \cdot b_w \cdot d$ $k_f = 1 - 10 \cdot \rho_{fw} \cdot \frac{E_{fw}}{E_c}; \quad \beta = 3 \cdot \frac{d}{a}; \quad k = 1 + \sqrt{200/d}$
Nehdi *et al.* [28]	$V_c = 2.1\left(\frac{f_c\rho_f d}{a} \star \frac{E_f}{E_s}\right)^{0.3} b_w d, \quad when\ \frac{a}{d} \ge 2.5$ $V_c = 2.1\left(\frac{f_c\rho_f d}{a} \star \frac{E_f}{E_s}\right)^{0.3} b_w d \cdot \frac{2.5d}{a}, \quad when\ \frac{a}{d} \le 2.5$
Design procedure – FRP (codes)	**Calculations**
The Japanese Society of Civil Engineers (JSCE) Method 1 [21]	$V_{cf} = \beta_d\beta_p\beta_n f_{vcd}bd/\gamma_b$ $f_{vcd} = 0.2(f'_{cd})^{1/3}$ $\beta_d = \left(\frac{1000}{d}\right)^{1/4} \le 1.5$ $\beta_p = \left(100\rho_f\frac{E_f}{E_s}\right)^{1/3} \le 1.5$ $\beta_n = 1 + \frac{M_o}{M_d} \quad for \quad N\_d \ge 0$ $\beta_n = 1 + \frac{M_o}{M_d} \quad for \quad N\_d < 0$ β_n should be within the limits: $1 \le \beta_n \le 2.0$ where: γ_b is the member safety factor = 1.3
The Japanese Society of Civil Engineers (JSCE) Method 2 [21]	$V_{cf} = \frac{\beta_{PEO}\beta_d(f'_{cd})^{\frac{1}{3}}(h-x)b}{\gamma_b}$ Where $\beta_d = \left(\frac{1000}{d}\right)^{\frac{1}{4}} \le 1.5$ $\beta_{PEO} = 0.17\left(\frac{\rho_f E_f}{5000} + 0.66\right) \le 0.28$
ACI Committee 440. Guide for the design construction of concrete reinforced with FRP bars. ACI440.1R-06. [20]	$V_{cf} = \frac{2}{5}\sqrt{f_c \star b_w \star k \star d}$ $k = \sqrt{2 \star n_f \star \rho_f + (n_f \star \rho_f)^2} - n_f \star \rho_f$ $\rho_f = \frac{A_f}{b_w d}; n_f = \frac{E_f}{E_c}; f_c \le 69$ MPa
CEN (Euro code 2) [23]	$V_{cf} = \left(C_{Rd,c} \star k(100 \star \rho_f \star f_c)^{\frac{1}{3}}\right)b_w d \quad V_{Rd,c} \ge v_{\min\, b_w d}$ $\rho_f = (A_f/b_w d) \star \left(\frac{E_f}{E_s}\right); k = 1 + \sqrt{\frac{200}{d}} \le 2.0$ $v_{min} = \frac{0.035}{\gamma_c=1} \star k^{\frac{3}{2}} \star f_c^{0.5}; C_{Rd,c} = \frac{0.18}{\gamma_c=1}$
CAN/CSA-S806-02 Code [24]	$V_{cf} = \left(\frac{130}{1000+d}\right)\lambda\varnothing_c\sqrt{f'_c}b_w d \ge 0.08\lambda\varnothing_c\sqrt{f'_c}b_w d$

V_{cf}: shear capacity of concrete beams without shear reinforcement, ρ: longitudinal reinforcement ratio, n: modular ratio, E_r: modulus of elasticity of reinforcement, b_w: width of the web in mm, c: cracked transformed section neutral axis depth in m, f_c: concrete compressive strength, d: effective depth, E_f: modulus of elasticity FRP, E_s: modulus of elasticity steel

Table 7: Shear capacity of concrete beams reinforced with steel bars without shear reinforcement

Design procedure-steel	Calculations
Zsutty Equation [25]	$V_c = 2.2\left(f_c\rho\frac{d}{a}\right)^{\frac{1}{3}}bd$
ACI 11-3 (ACI 2008) [26]	$V_c = \left(\frac{\sqrt{f'_c}}{6}\right)b_w d$
Bazant Equation [29]	$V_c = \left[0.54\sqrt[3]{\rho}\left(\sqrt{f'_c} + 249\sqrt{\frac{\rho}{\left(\frac{a}{d}\right)^5}}\right) \star \frac{1+\sqrt{\frac{5.08}{d_o}}}{\sqrt{1+\frac{d}{25d_o}}}\right] b_w d$
ACI 11-5 (ACI 2008) [26]	$V_c = \left(0.158\sqrt{f_c} + 17\rho \star \frac{V_u}{M_u}\right)bd \le 0.3\sqrt{f'_c}bd$ *Where* $V_u d/M_u \le 1.0$
Eurocode draft (2003) [23]	$V_c = 0.12k\left(100\rho f'_c\right)^{\frac{1}{3}}bd$ *where* $k = 1 + \sqrt{200/d} \le 2.0$, $\rho \le 0.02$
Tureyen and Frosch (2003) [25]	$V_c = \frac{5}{12}\sqrt{f'_c}bc$ *where* $c = kd$, $k = \sqrt{2\rho n + (\rho n)^2} - \rho n$ and $n = E_s/E\_c$
Bazant and Yu (2005) [32]	$V_c = 1.1044\rho^{\frac{3}{8}}b\left(1 + \frac{d}{a}\right)\sqrt{\frac{f'_c d_0 d}{1+\frac{d_0}{d}}}$ where $d_0 = k\left(f'_c\right)^{-2/3}$, and $k = 693.7623\sqrt{d_0}$
Russo *et al.* [33] (2005)	$V_c = 1.13\zeta\left[\rho^{0.4}\left(f'_c\right)^{0.39} + 0.5\rho^{0.83}f_y^{0.89}\left(\frac{a}{d}\right)^{-1.2-0.45\left(\frac{a}{d}\right)}\right]bd$ *where* $\zeta = \frac{1+\sqrt{5.08/d_0}}{\sqrt{1+d/(25d_0)}}$

5.3 Available equations and design recommendations

Tables 6 and 7 show some of the available equations for evaluating the concrete shear strength of concrete members longitudinally reinforced with FRP bars and reinforced with steel bars are presented here. These equations were proposed by researchers or stated by design recommendations.

5.4 Proposed method for determining the shear strength of FRP reinforced concrete members without stirrups

From total experimental work, the proposed theoretical equation for calculated shear forces is as follows:

$$V = V_C + V_a + V_d \tag{4}$$

V_C – the contribution from uncracked (plain) concrete
V_a – the contribution from the aggregate interlock mechanism
V_d – the contribution from dowel action.

The proposed method is an improved version of the existing CSA S806-02 or proposed equation of fracture mechanics as give the same results to calculate (V_c and V_a)

$$V_c = 0.035k_m k_s k_a\sqrt{f'_c}b_w d \tag{5}$$

$$V_a = 0.035k_m k_s k_a k_r\sqrt{f'_c}b_w d \tag{6}$$

$$V_c + V_a = 0.035k_m k_s k_a\left(1 + k_r\right)\sqrt{f'_c}b_w d \le 0.2k_s\sqrt{f'_c}b_w d \tag{7}$$

where k_m represents the effect of interaction between the factored moment and the factored shear at the section on its shear strength; k_r represents the effect of reinforcement rigidity ($\rho_f E_f$, $\rho_s E_s$); and k_a and k_s represent the effects of arch action and beam size, respectively. These factors are given as follows

$$k_m = \left(\frac{V_F d}{M_F}\right)^{2\backslash 3} \tag{8}$$

where $\left(\frac{M_f}{V_f d}\right)$ is the same ($a\backslash d$)

$$k_r = \left(\rho_f E_f + \rho_s E_s\right)^{\frac{1}{3}} \tag{9}$$

$$k_a = 1 \quad \text{for} \quad \frac{M_F}{V_F d} \ge 2.5 \tag{10}$$

$$k_a = \frac{2}{\left(\frac{M_F}{V_F d}\right)} \le 2.5 \quad \text{for} \quad \frac{M_F}{V_F d} < 2.5 \tag{11}$$

$$k_s = 1 \quad \text{for} \quad d \le 300 \tag{12}$$

Table 8: The comparison between theoretical and experiential results

Specimen no	h (mm)	Reinf. Steel	Reinf. GFRP	AS′	a/d	f_c (Mpa)	$V_C + V_a$	V_d	$V_{the} = V_c + V_a + V_d$	$V_{\exp(p/2)}$	$\frac{V_{\exp}}{V_{theor}}$
B4	300	2ϕ10	2#3	2ϕ12	2.67	25	61.93	5.93	67.86	67.84	1.0
B5	300	2ϕ12	2#4	2.67	25	69.54	6.9	76.44	73.2	0.96	
B6	300	2ϕ16	2#5	2.67	25	87.93	8.75	96.68	105.7	1.09	
B7	200	2ϕ12	2#4	2.67	25	51.14	6.9	58.04	65	1.12	
B8	400	2ϕ12	2#4	2.67	25	89.82	6.9	96.72	99.3	1.02	
B9	300	2ϕ12	2#4	2.0	25	77.35	6.9	84.25	75.6	0.90	
B10	300	2ϕ12	2#4	3.0	25	59.03	6.9	65.93	59.8	0.91	
B11	300	2ϕ12	2#4	3.5	25	53.27	6.9	60.17	53.4	0.89	
B12	300	2ϕ12	2#4	2.67	30	76.18	6.9	83.08	78.9	0.95	
B13	300	2ϕ12	2#4	2.67	40	87.96	6.9	94.86	103.2	1.08	
B14	300	2ϕ12	2#4	2.67	50	98.34	6.9	105.24	126.4	1.20	

$$= \left(\frac{750}{450 + d}\right) * 1.15 \quad \text{for} \quad d \geq 300 \tag{13}$$

To calculate (V_d) use an improved equation of Jimenez, Gergely, and White:

$$V_d = \left[\frac{b_n d_b^*}{n_b}\left(3.25 + \frac{3.79 c_m}{\frac{b_n}{n_b^2} + d_b}\right)\right] \tag{14}$$

Where b_n: is the net width of the beam $(b - n\varnothing)$, n_b is the number of bars in one layer, c_m is the minimum cover (side or bottom)
d_b^* is the bar diameter of bars equal to:

$$d_b^* = d_{fiber} * \frac{E_F}{E_S} + d_{steel} \tag{15}$$

$$V = 0.035 k_m k_s k_a (1 + k_r)\sqrt{f_c'} b_w d + \left[\frac{b_n d_b^*}{n_b}\left(3.25 + \frac{3.79 c_m}{\frac{b_n}{n_b^2} + d_b}\right)\right]$$

As shown in Table 8, the theoretical Eqs. (4–5) gives acceptable results compared with the experiment work and can be used as a guide equation for the prediction of the shear strength of hybrid GFRP/steel of reinforced concrete beams without shear reinforcement.

6 Conclusions

Based on the analysis of the experimental results of the tested RC beams in this work, the following conclusions can be drawn

- Using hybrid GFRP/steel bars in RC beams causes a reduction in the cracking loads, also decreased number and width cracks, crack width increased compared to using GFRP only in RC beams.
- Using hybrid GFRP/steel bars decreased deflection with a ratio of 30% and increased ductility 16% for beams reinforced with pure fiber
- Using hybrid GFRP/steel bars decreased deflection and increased ductility for beams reinforced with steel so we can say GFRP/steel enhance ductility
- Using variable span- to- depth ratio (2, 2.67, 3 and 3.5) we conclusion a/d equals 2 is the best ratio because it gave good results of stiffness, ductility, ultimate loads, and decreased strain in bars compared to other ratios, also increasing concrete strength increased the ultimate load, stiffness, delayed the cracking loads.
- The sound of failure of hybrid beams such as beams reinforced with steel bars but no sound occurs during failure on beams reinforced with GFRP only
- cracks and mode of failure in hybrid beams are closer to beams with steel bars than to beams reinforced with GFRP only.
- Most of the main GFRP/steel bars exceed the yield strain so the main tension bar plays an important role in resisting the ultimate load, the failure together with using hybrid reduces the strain in bars compared with using fiber.
- Based on shear transfer mechanisms, and numerous published experimental data, the following equation is derived for the nominal shear strength of hybrid in reinforced concrete beams without web reinforce-

ment

$$V = 0.035 k_m k_s k_a (1 + k_r) \sqrt{f'_c} b_w d + \left[\frac{b_n d_b^*}{n_b} \left(3.25 + \frac{3.79 c_m}{\frac{b_n}{n_b^2} + d_b} \right) \right]$$

- Comparison with published experimental data indicates that the proposed equation estimates properly the effects of primary factors, such as concrete strength, longitudinal hybrid bars ratio, shear span-to-depth ratio, and effective depth.

Funding information: The authors state no funding involved.

Author contributions: All authors have accepted responsibility for the entire content of this manuscript and approved its submission.

Conflict of interest: The authors state no conflict of interest.

References

[1] Rizkalla S, Hassan T, Hassan N. Design recommendations for the use of FRP for reinforcement and strengthening of concrete structures. Prog Struct Eng Mater. 2003;5(1):16–28.

[2] Pang L, Qu W, Zhu P, Xu J. Design propositions for hybrid FRP-steel reinforced concrete beams. J Compos Constr. 2016;20(4):04015086.

[3] Aiello MA, Ombres L. Structural performances of concrete beams with hybrid (fiber-reinforced polymer-steel) reinforcements. J Compos Constr. 2002;6(2):133–140.

[4] Masmoudi R, Theriault M, Benmokrane B. Flexural behavior of concrete beams reinforced with deformed fiber reinforced plastic reinforcing rods. ACI Struct J. 1998;95(6):665-676.

[5] Kocaoz S, Samaranayake VA, Nanni A. Tensile characterization of glass FRP bars. Compos B Eng. 2005;36(2):127-134. https://doi.org/10.1016/j.compositesb.2004.05.004.

[6] Nguyen PD, Dang VH, Vu NA. Performance of concrete beams reinforced with various ratios of hybrid GFRP/steel bars. Civ Eng J. 2020;6(9):1–18.

[7] Bakis CE, Nanni A, Terosky JA, Koehler SW. Self-monitoring, pseudo-ductile, hybrid FRP reinforcement rods for concrete applications. Compos Sci Technol. 2001;61(6):815–23.

[8] Qu W, Zhang X, Huang H. Flexural behavior of concrete beams reinforced with hybrid (GFRP and steel) bars. J Compos Constr. 2009;13(5):350–9.

[9] Bakis CE, Nanni A, Terosky JA. Smart, pseudo-ductile, reinforcing rods for concrete: manufacture and test. First International Conference on Composites in Infrastructure. 1996 Jan 15-17; Tuscon (AZ), USA. 1996. p. 95-108.

[10] De Domenico D, Pisano AA, Fuschi P. A FE-based limit analysis approach for concrete elements reinforced with FRP bars. Compos Struct. 2014;107:594–603.

[11] Jaejer LG, Mufti AA, Tadros G. The concept of the overall performance factor in rectangular-section reinforced concrete beams. Proceedings of the 3rd International Symposium on Non-Metallic (FRP) Reinforcement for Concrete Structures. 1997 Oct 14-16; Sapporo, Japan. Tokyo: Japan Concrete Institute; 1997. p. 551–559.

[12] Rousakis TC, Saridaki ME, Mavrothalassitou SA, Hui D. Utilization of hybrid approach towards advanced database of concrete beams strengthened in shear with FRPs. Compos B Eng. 2016;85:315–35.

[13] Tottori S, Wakui H. Shear capacity of RC and PC beams using FRP reinforcement. ACI Symposium Paper. 1993;138:615–632.

[14] Zhao W, Maruyama K, Suzuki H. Shear behavior of concrete beams reinforced by FRP rods as longitudinal and shear reinforcement. Proceedings of the 2nd International Symposium on Non-Metallic (FRP) Reinforcement for Concrete Structures. 1995 Aug 23-25; Ghent, Belgium. London, New York: E & FM Spon; 1995. p. 352–352.

[15] Tureyen A. Koray; Frosch, Robert J. Shear tests of FRP-reinforced concrete beams without stirrups. ACI Struct J. 2002;99(4):427–34.

[16] Razaqpur AG, Isgor BO, Greenaway S, Selley A. Concrete contribution to the shear resistance of fiber reinforced polymer reinforced concrete members. J Compos Constr. 2004;8(5):452–60.

[17] Razaqpur AG, Isgor OB. Proposed shear design method for FRP-reinforced concrete members without stirrups. ACI Struct J. 2006;103(1):93–102.

[18] ACI Committee 318. Building code requirements for reinforced concrete (ACI 318-02) and commentary (ACI 318R-02). Farmington Hills (MI): American Concrete Institute; 2002. p. 443.

[19] ACI Committee 440. Guide for the design and construction of concrete reinforced with FRP bars (ACI 440.1R-01). Farmington Hills (MI): American Concrete Institute; 2001. p. 41.

[20] ACI Committee 440. Guide for the design and construction of concrete reinforced with FRP bars (ACI 440). Farmington Hills (MI): American Concrete Institute; 2006. p. 44 .

[21] Japanese Society of Civil Engineers JSCE. Recommendation for design and construction of concrete structures using continuous fiber reinforcing materials. In: Machida A, editor. Concrete Engineering Series 3. 1997. p. 164.

[22] Canadian Standard Association (CSA). Design and construction of building components with fibre- reinforced polymers. Ontario, Canada: Canadian Standard S806-02. 2002.

[23] Eurocode 2: Design of concrete structures- Part 1–1: General rules and rules for buildings. London, UK: British Standard Institution. 2005.

[24] Canadian Standard Association (CSA) Supplement #1 to CAN/CSA-S6-06, Canadian Highway Bridge Design Code. Ontariu, Canada: Canadian Standard S6S1-10. 2010.

[25] Tureyen AK, Frosch RJ. Concrete shear strength: another perspective. ACI Struct J. 2003;100(5):609–15.

[26] Jung S, Kim KS. Knowledge-based prediction of shear strength of concrete beams without shear reinforcement. Eng Struct. 2008;30(6):1515–25.

[27] Hegger J, Niewels J, Kurth M. Shear analysis of concrete members with Fiber-Reinforced Polymers (FRP) as internal reinforcement. In: Oehlers DJ, Griffith MC, Seracino R, editors. Proceedings of the 9th International Symposium on Fiber-Reinforced Polymer Reinforcement for Concrete Structures (FRPRCS-9). 2009 Jul 13-15; Sydney, Australia, 2009.

[28] Nehdi M, El Chabib H, Aly Said A. Proposed shear design equations for FRP-reinforced concrete beams based on genetic algorithms approach. J Mater Civ Eng. 2007;19(12):1033–42.
[29] Kim JK, Park YD. Prediction of shear strength of reinforced concrete beams without web reinforcement. ACI Mater J. 1996;93(3):213–222.
[30] Budvytis M, Escamilla AC, Juknevičius L. Analysis of shear design recommendations for FRP reinforced concrete beams. Eng Sci Technol. 2018;10(2):46–57.
[31] Song JH, Kang WH, Kim KS, Jung SM. Probabilistic shear strength models for reinforced concrete beams without shear reinforcement. Struct Eng Mech. 2010;34(1):15–38. https://doi.org/10.12989/sem.2010.34.1.015.
[32] Bažant ZP, Yu Q. Designing against size effect on shear strength of reinforced concrete beams without stirrups: I. Formulation. J Struct Eng. 2005;131(12):1877–85.
[33] Russo G, Somma G, Mitri D. Shear strength analysis and prediction for reinforced concrete beams without stirrups. J Struct Eng. 2005;131(1):66–74.
[34] Matta F, Nanni A, Galati N, Mosele F. Size effect on shear strength of concrete beams reinforced with FRP bars. Proceedings of the 6th International Conference on Fracture Mechanics of Concrete and Concrete Structures (FraMCoS-6). 2007 Jun 17-22; Catania, Italy. 2007.
[35] Krefeld W, Thurston CW. Contribution of longitudinal steel to shear resistance of reinforced concrete beams. ACI J Proc. 1966;63:325–344.
[36] Taylor HP. Investigation of the dowel shear forces carried by the tensile steel in reinforced concrete beams. London, UK: Cement and Concrete Association. 1969.
[37] Houde J, Mirza MS. A finite element analysis of shear strength of reinforced concrete beams. ACI Symposium Paper. 1974;42:103–128.
[38] Jimenez-Perez R, Gergeley P, White RN. Shear transfer across cracks in reinforced concrete. Cornell University, USA. 1978.
[39] Baena M, Torres L, Turon A, Barris C. Experimental study of bond behaviour between concrete and FRP bars using a pull-out test. Compos B Eng. 2009;40(8):784–97.
[40] Tighiouart B, Benmokrane B, Gao D. Investigation of bond in concrete member with fiber reinforced polymer (FRP) bars. Constr Build Mater. 1998;12(8):453–62.
[41] Autrup F, Jørgensen HB, Hoang LC. Experimental investigation of dowel action in RC beams without shear reinforcement. fib Symposium 2020. 2020 Nov 22-25; Shanghai, China. 2020.
[42] Mazaheripour H, Barros JA, Sena-Cruz JM, Pepe M, Martinelli E. Experimental study on bond performance of GFRP bars in selfcompacting steel fiber reinforced concrete. Compos Struct. 2013;95:202–12.
[43] Gustafsson PJ, Hillerborg A. Sensitivity in shear strength of longitudinally reinforced concrete beams to fracture energy of concrete. ACI Struct J. 1988;85(3):286–94.
[44] Jenq YS, Shah SP. Shear Resistance of Reinforced Concrete Beams-A Fracture Mechanics Approach. ACI Symposium Paper. 1989;118:237–58.
[45] So KO; Karihaloo BL. Shear Capacity of Longitudinally Reinforced Beams—A Fracture Mechanics Approach. ACI Mater J. 1993;90(6):591–600.
[46] Gastebled OJ, May IM. Fracture mechanics model applied to shear failure of reinforced concrete beams without stirrups. ACI Struct J. 2001;98(2):184–90.

Appendix: A

A Behavior prediction using nonlinear finite-element analysis

The finite element method is a numerical analysis technique that can be used to obtain approximate solutions to a wide range of engineering problems. ANSYS is a general-purpose finite element modeling package that can be used to solve a wide variety of problems, including heat transfer, static and dynamic structural analysis (both linear and non-linear), and fluid problems. The Hybrid GFRP/Steel Bars in Reinforced Concrete Beams without shear reinforcement have been analyzed using a finite element (FE) model in ANSYS. The 'ANSYS' model accounts for cracks, strain in bars, deflection, and stress transfer across the cracked blocks of the concrete. The study was performed with the Newton-Raphson technique in stages. The final results are applied after the solution has been converged.

A.1 Modeling of concrete and reinforcement

SOLID65, defined as an eight-node brick element capable of simulating the cracking and crushing of brittle materials, was used to model the concrete. The compressive and tensile strengths are determined using test data from specimens cast and examined along with the rectangular beams. The data was used in 'ANSYS' to define concrete ('CONCR') properties. Concrete is considered to be anisotropic elastic material before crushing. The concrete is believed to have lost hardness in all directions after crushing. The concrete Poisson's ratio is 0.2 A constant mesh size of 50mm is assumed in this study. The meshed solid is presented in Figure 10. The longitudinal reinforcement i.e., the steel and fiber bars have been modeled using LINK8 3D Spar element. The 3-D spar element is a uniaxial tension-compression element with three degrees of freedom at each node: nodal x, y, and z translations with significant deflection capabilities. The area equivalent to each rebar is used to calculate the cross-sectional area of each element. For the rebar, the same mesh size as that of a concrete element is adopted. Figure 10 shows a typical beam modeled in ANSYS.

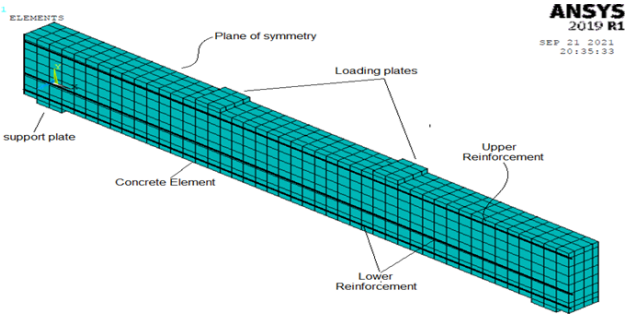

Figure 10: Element Types of ANSYS Modelling

A.2 Discussion on test results

A.2.1 Crack pattern

The first crack observed in the shear span during the testing of the beam was found to be similar in the ANSYS predicted model. Cracks propagated through the moment zone at higher loads in further stages of loading of the ANSYS predicted model. The orientations of cracks predicted by the model are inclined in the shear span region and vertical in the constant moment region. The crack patterns and the order of cracks predicted by the ANSYS model are in confirming with experimental observations. During the test process, at ultimate load, the inclined crack in shear span widened and concrete under the load point crushed. The ANSYS model predicted the crushing of concrete at ultimate by indicating large distortion of element nodes. The crack patterns indicate shear failure in all beams. The crack pattern observed in the ANSYS model at failure is illustrated in Figure 11.

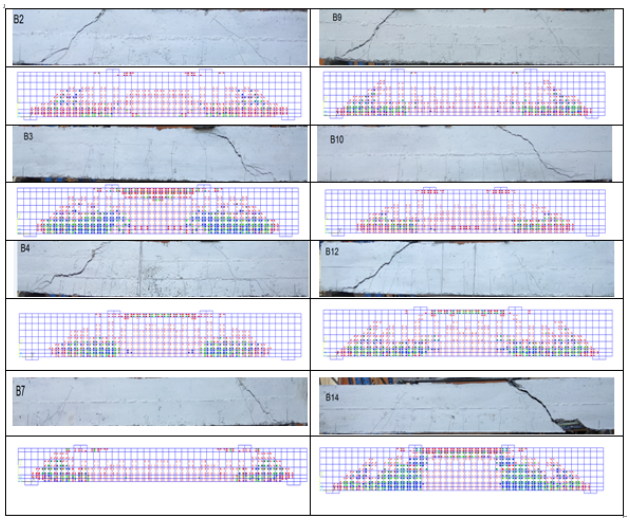

Figure 11: Comparison between crack pattern from (F.E.) and experimental test for specimens

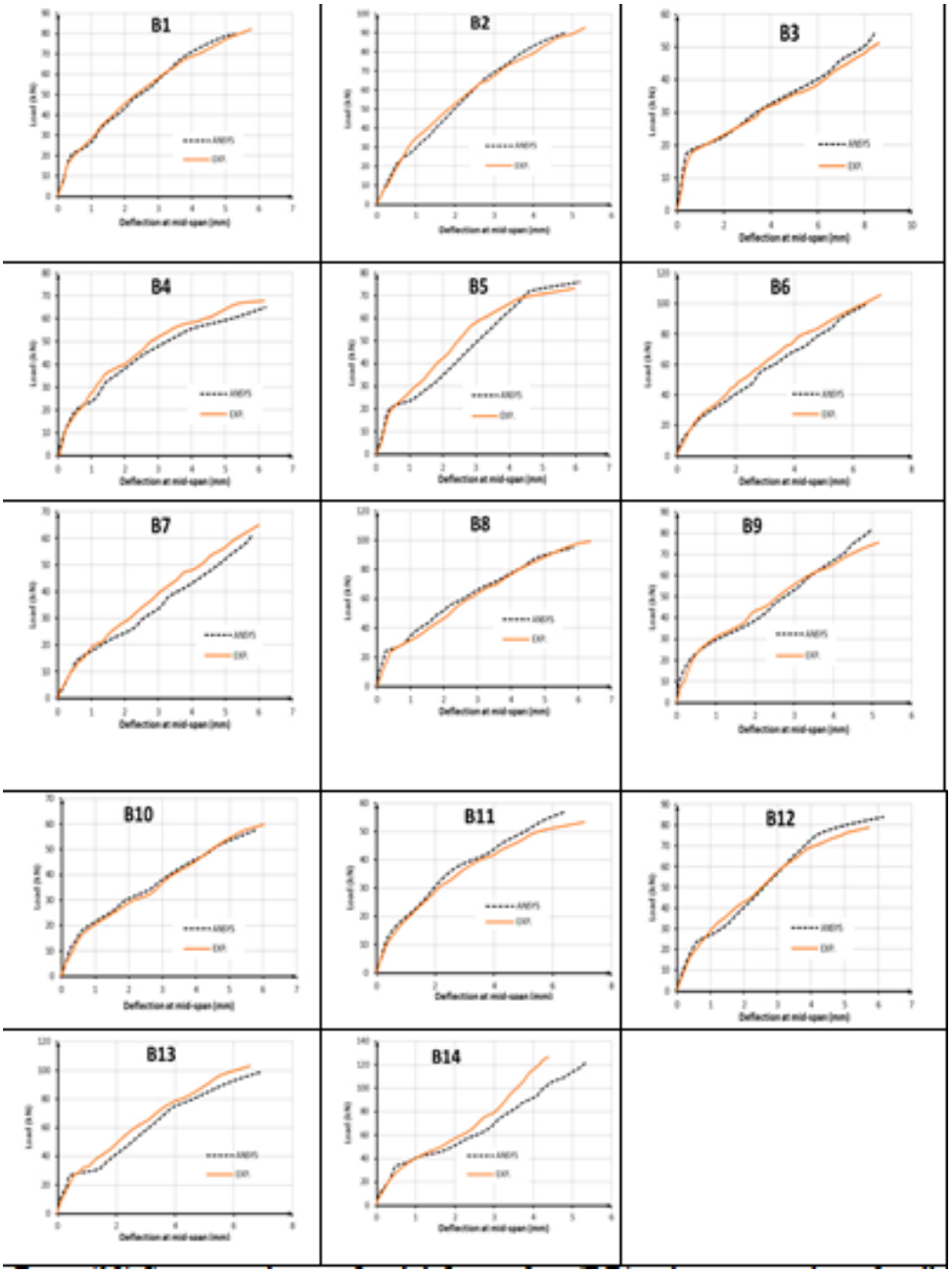

Figure 12: Comparison between Load-deflection from (F.E.) and experimental test for all specimens

A.2.2 Load-deflection curves

Theoretical (FEM-ANSYS) and the experimental mid-span deflection is calculated and obtained from the same location on the tested beam. The load-deflection curves from the FEM and the experimental results for beam specimens are shown in Figure 12. The predicted load-deflection curves show good agreement with that from experimental work.

Table 9 lists the analytical and experimental ultimate loads. The findings demonstrated that the method had predicted the ultimate strength of the test specimens successfully. Because the average difference between the ultimate deflection and the experimental ultimate loads and their numerical simulated values was less than 5%. Furthermore, the ratios between ultimate deflection and the experimental ultimate loads and their numerical simulated values indicate an acceptable simulation. As a result, we can say that the ANSYS response complements the experimental results.

Table 9: Experimental and predicted, first cracking load, ultimate load capacity, and ultimate deflection for all tested specimens

Beam No.	Experemental First cracking load (MPa)	Predicted First cracking load (MPa)	(Experimental/ predicted) First cracking load (MPa)	Pu(exp) [kN]	Pu(ANSYS) [kN]	Pu(exp) [kN]/ Pu(ANSYS)	Δu(exp) [mm]	Δu(ANSYS) [mm]	Δu(exp)/ Δu(ANSYS)
B1	39.5	28	1.4	82.2	80	1.027	5.771	5.261	1.096
B2	64.5	40	1.6	92.8	90	1.03	5.319	4.799	1.108
B3	17.5	14	1.25	51.3	54	0.95	8.609	8.403	1.024
B4	21.84	15	1.45	67.84	65	1.04	6.164	6.203	0.99
B5	37.4	27	1.38	73.2	76	0.96	5.951	6.101	0.975
B6	40.7	32	1.27	105.7	99	1.067	6.948	6.411	1.083
B7	48.2	35	1.37	65	61	1.065	5.996	5.786	1.036
B8	41.3	25	1.65	99.3	95	1.045	6.37	5.846	1.089
B9	37.7	25	1.5	75.6	82	0.92	5.154	4.988	1.03
B10	24.8	18	1.38	59.8	58	1.03	6.018	5.829	1.032
B11	23.7	15	1.58	53.4	57	0.936	7.067	6.406	1.10
B12	40.5	26	1.56	78.9	84	0.939	5.73	6.154	0.93
B13	49	30	1.63	103.2	99	1.042	6.545	6.927	0.94
B14	64.8	40	1.62	122	123.1	0.99	4.804	5.321	0.90